

Asymptotic Limit-cycle Analysis of the FitzHugh-Nagumo Equations

Alain J. Brizard

Department of Physics, Saint Michael's College, Colchester, VT 05439, USA

(Dated: July 27, 2021)

The asymptotic limit-cycle analysis of the FitzHugh-Nagumo equations is presented. In this work, we obtain an explicit analytical expression for the relaxation-oscillation period that is accurate within 1% of their numerical values. In addition, we derive the critical parametric values leading to canard explosions and implosions in its associated limit cycles.

I. INTRODUCTION

The FitzHugh-Nagumo (FHN) equations [1–3] provide a simple model describing the activation and deactivation of spiking behavior in neurons. Nagumo [2] introduced an electric-circuit representation of the FitzHugh [1] model, in which a three-segment parallel circuit is built from a capacitor C in one segment, in parallel with a tunnel diode (with an emf \mathcal{E}_0) in a second segment, and an LR -segment with a resistor R connected in series with an inductor L .

The Kirchhoff junction equation for the Nagumo circuit is expressed as the sum of three currents equal to the constant external current I that flows into the three-segment junction:

$$I = I_C + I_D(\varepsilon) + I_R, \quad (1)$$

where I_C is the capacitor current, $I_D(\varepsilon)$ is the diode current (which depends on the potential difference ε across the diode), and I_R is the current flowing through the LR segment.

By denoting the potential difference across each segment as V , we obtain the capacitor current $I_C = C dV/dt$, and the LR current I_R yields the relation

$$V = RI_R + L dI_R/dt. \quad (2)$$

Lastly, we define the potential difference across the tunnel diode as $\varepsilon = V - \mathcal{E}_0$, so that the tunnel-diode current is modeled as

$$I_D(\varepsilon) = I_0 - \frac{\Delta\varepsilon}{R_0} \left[\left(\frac{\varepsilon - \varepsilon_0}{\Delta\varepsilon} \right) - \frac{1}{3} \left(\frac{\varepsilon - \varepsilon_0}{\Delta\varepsilon} \right)^3 \right], \quad (3)$$

where I_0 flows through the diode when the potential difference is ε_0 , which defines the negative resistance $1/I_D'(\varepsilon_0) = -R_0 < 0$. The potential differences $\varepsilon_0 \pm \Delta\varepsilon$, on the other hand, are used to define the maximum and minimum $I_D(\varepsilon_0 \mp \Delta\varepsilon) = I_0 \pm \frac{2}{3} \Delta\varepsilon/R_0$ of the tunnel-diode current (3).

By introducing the following dimensionless variables: the diode potential $x = (\varepsilon - \varepsilon_0)/\Delta\varepsilon$ and the resistor current $y = (I_0 + I_R)R_0/\Delta\varepsilon$, the Kirchhoff junction equation (1) becomes

$$c = \dot{x} + x^3/3 - x + y, \quad (4)$$

where $c = IR_0/\Delta\varepsilon$ is the negative-resistance parameter, and we introduced the dimensionless time derivative

$\dot{x} = R_0C dx/dt$, which is normalized to the R_0C time constant. This equation is coupled to the resistor-current equation (2), now written in dimensionless form as

$$x = by - a + \epsilon^{-1} \dot{y}, \quad (5)$$

where $a = (RI_0 + \varepsilon_0 + \mathcal{E}_0)/\Delta\varepsilon$ and $b = R/R_0$ are arbitrary constants, and the small dimensionless parameter is $\epsilon = \omega^2(R_0C)^2 \ll 1$, where $\omega = 1/\sqrt{LC}$ is the natural LC frequency (i.e., the LC period is chosen to be much longer than the R_0C time constant).

There is a large amount of literature on the FHN equations and its extensions [3]. As a simplification of the four-variable Hodgkin-Huxley model [4], the FHN model [2] combines: (1) the membrane potential V and the sodium activation variable m as the membrane potential variable x ; (2) the sodium inactivation variable h and the potassium activation parameter n as the recovery variable y ; and (3) the membrane current is represented by the stimulus current c . Like the Van der Pol paradigm [5], these equations display a Hopf bifurcation at a critical value of the control parameter c , where a stable fixed point is replaced by a stable limit cycle. Once a stable limit cycle is created, a sudden transition from a small-amplitude oscillation to a large-amplitude relaxation oscillation is described as a canard explosion.

The remainder of the paper is organized as follows. In Sec. II, we present the mathematical preliminary material that underlies the stability, bifurcation, and canard analysis of coupled first-order differential equations. In particular, we present the Fenichel geometric singular perturbation theory [6, 7], which is applied to the Van der Pol equations. In Sec. III, we apply this analysis to the FHN equations, which yields an explicit analytical expression for the relaxation-oscillation period that is accurate within 1% of their numerical values, as well as critical parametric values leading to canard explosions and implosions in its associated limit cycles.

II. MATHEMATICAL PRELIMINARIES

The FHN equations (4)-(5) are generically expressed as the nonlinear singular first-order ordinary differential equations

$$\left. \begin{aligned} \dot{x} &= F(x, y; a) \\ \dot{y} &= \epsilon G(x, y; a) \end{aligned} \right\}, \quad (6)$$

where x and y denote dimensionless dynamical variables, and each dimensionless time derivative is represented with a dot (e.g., $\dot{x} = dx/dt$). On the right side of Eq. (6), the dimensionless parameter ϵ plays an important role in the qualitative solutions of Eq. (6), while the functions $F(x, y; a)$ and $G(x, y; a)$ (which may depend on a dimensionless control parameter a) are used to define the nullcline equations: $F(x, y; a) = 0 = G(x, y; a)$, which yield separate curves $y = f(x; a)$ and $y = g(x; a)$ onto the (x, y) -plane. A simplifying assumption used here is that the functions F and G are at most separately linear in y and a , with $\partial^2 F/\partial y \partial a = 0 = \partial^2 G/\partial y \partial a$.

By introducing a new time normalization $t' = \epsilon t$, the equations (6) may also be written as

$$\left. \begin{aligned} \epsilon x' &= F(x, y; a) \\ y' &= G(x, y; a) \end{aligned} \right\}, \quad (7)$$

where a prime now denotes a derivative with respect to t' (e.g., $x' = dx/dt'$). According to standard terminology, the times t' and t are called the slow time and fast time, respectively, and Eqs. (6) and (7) are called the fast system and slow system, respectively.

We note that the slope function $m(x, y; a) \equiv \dot{y}/\dot{x} = y'/x' = \epsilon G(x, y; a)/F(x, y; a)$ is a useful qualitative tool as we follow an orbit in the $y(t)$ -versus- $x(t)$ phase space. In particular, we see that the orbit crosses the y -nullcline horizontally ($m = 0$) while it crosses the x -nullcline vertically ($m = \pm\infty$). Hence, in the limit $\epsilon \ll 1$, the slope function is near zero (i.e., the orbit is horizontal) unless the orbit is near the x -nullcline, where $F(x, y; a) \simeq 0$. As the slope $m(x, y; a)$ depends on the model parameter a , the shape of the orbit solution will also change with a .

The dynamical equations (6) can exhibit a type of large-amplitude oscillations called relaxation oscillations [8]. The paradigm for these large-amplitude oscillations is represented by the biased Van der Pol equation [9]

$$\frac{d^2 x}{dt^2} - \nu(1 - x^2) \frac{dx}{dt} + \omega^2 x = \omega^2 a, \quad (8)$$

where ω is the natural frequency of the linearized harmonic oscillator and ν is the negative dissipative rate, while the bias parameter a represents an equilibrium value of the dimensionless oscillator displacement x . We note that the term $-\nu(1 - x^2) dx/dt$ yields negative dissipation in the range $x^2 < 1$, which leads to exponential growth in that range.

From Eq. (8), we obtain the coupled dimensionless equations

$$\left. \begin{aligned} \dot{x} &= x - x^3/3 - y \\ \dot{y} &= \epsilon(x - a) \end{aligned} \right\}, \quad (9)$$

where the dimensionless time is normalized to ν^{-1} (i.e., $\dot{x} = \nu^{-1} dx/dt$) and $\epsilon \equiv \omega^2/\nu^2$ [10]. Here, the x -nullcline is $y(x) = x - x^3/3$ (which has a minimum at $x = -1$ and a maximum at $x = 1$) while the y -nullcline is a vertical line at $x = a$.

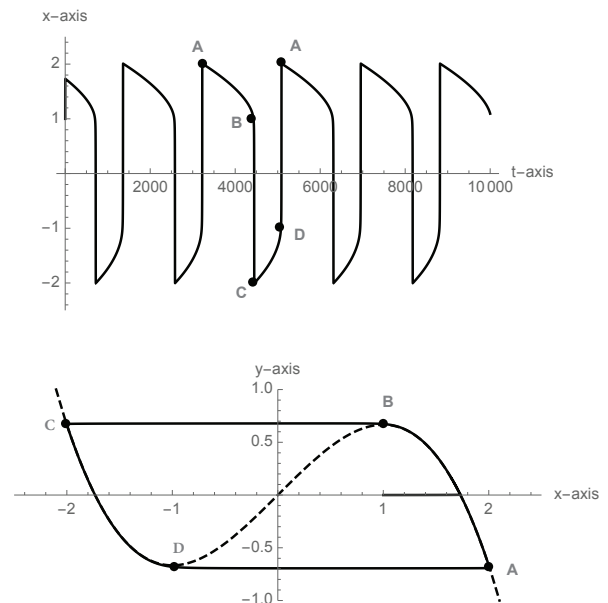


FIG. 1: Relaxation oscillation in the Van der Pol equations for $a = 0.5$ and $\epsilon = 0.001$. (Top) Plot of $x(t)$ versus time t and (Bottom) Phase-space portrait showing $y(t)$ versus $x(t)$, with the x -nullcline shown as a dashed curve.

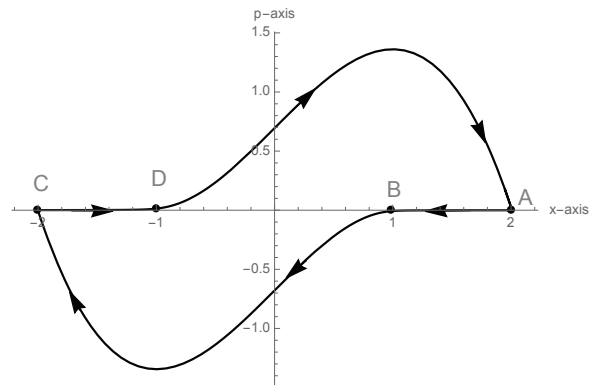


FIG. 2: Phase-space plot $p(t) \equiv \dot{x}(t) = x(t) - \frac{1}{3}x^3(t) - y(t)$ versus $x(t)$ for the relaxation oscillation shown in Fig. 1. Here, $y(t) \simeq x(t) - \frac{1}{3}x^3(t)$, i.e., the orbit is near the x -nullcline, when $p(t) \simeq 0$ from A to B and C to D.

Figure 1 shows the solution of the Van der Pol equations (9) for $a = 0.5$ and $\epsilon = 0.001$ and the initial conditions $x(0) = 1$ and $y(0) = 0$. In the top plot, the solution $x(t)$ shows slow orbits (on time scales of order ϵ^{-1}) from A to B and C to D, and fast (exponential) transitions (on time scales of order ϵ^α , with $-1 < \alpha < 0$) from B to C and D to A. The bottom plot in Fig. 1 shows that the slow orbits occur near the x -nullcline (shown as a dashed curve). Figure 2, on the other hand, shows that the orbits from B to C and D to A include nonlinear exponential accelerations from ± 1 to ∓ 1 , respectively, and then nonlinear exponential decays from ∓ 1 to the turning points

$x_C \simeq -2$ and $x_A \simeq 2$, respectively.

A. Linear stability analysis

If the nullcline curves of Eq. (6) intersect at (x_0, y_0) , where $x_0 = x_0(a)$ and $y_0(a) = f(x_0) = g(x_0)$, the point (x_0, y_0) is called a fixed point of Eq. (6). The stability of this fixed point is investigated through a standard normal-mode analysis [8], where $x = x_0 + \delta\bar{x} \exp(\lambda t)$ and $y = y_0 + \delta\bar{y} \exp(\lambda t)$ are inserted into Eq. (6) to obtain the linearized matrix equation

$$\begin{pmatrix} \lambda - F_{x0} & -F_{y0} \\ -\epsilon G_{x0} & \lambda - \epsilon G_{y0} \end{pmatrix} \cdot \begin{pmatrix} \delta\bar{x} \\ \delta\bar{y} \end{pmatrix} = 0, \quad (10)$$

where the constant eigenvector components $(\delta\bar{x}, \delta\bar{y})$ are non-vanishing only if the determinant of the linearized matrix vanishes. Here, (F_{x0}, F_{y0}) and (G_{x0}, G_{y0}) are partial derivatives evaluated at the fixed point (x_0, y_0) and the eigenvalues $\lambda_{\pm} = \frac{1}{2} \tau \pm \frac{1}{2} \sqrt{\tau^2 - 4 \Delta}$ are roots of the quadratic characteristic equation $\lambda^2 - \tau \lambda + \Delta = 0$, where $\tau(a, \epsilon) \equiv F_{x0} + \epsilon G_{y0} = \lambda_+ + \lambda_-$ and $\Delta(a, \epsilon) = \epsilon (F_{x0} G_{y0} - F_{y0} G_{x0}) = \lambda_+ \cdot \lambda_-$ are the trace and determinant of the Jacobian matrix, respectively.

The fixed point is a stable point ($\tau < 0$ and $\Delta > 0$) that is either a node ($\tau^2 > 4 \Delta$), when the eigenvalues are real and negative: $\lambda_- < \lambda_+ < 0$, or a focus ($\tau^2 < 4 \Delta$), when the eigenvalues are complex-valued ($\lambda_- = \lambda_+^*$) with a negative real part. Otherwise, the fixed point is either an unstable point ($\tau > 0$ and $\Delta > 0$) or a saddle point ($\Delta < 0$). Periodic solutions of Eq. (6) exist when a Hopf bifurcation [8] replaces an unstable fixed point with a stable limit cycle, which forms a closed curve in the (x, y) -plane. Here, a limit cycle appears when the x -nullcline function $f(x; a)$ has non-degenerate minimum and maximum points and it is stable whenever the trace $\tau(a) > 0$ is positive in the range $a_s < a < a_u$.

For the Van der Pol equations (9), we easily find the fixed point $(x_0, y_0) = (a, a - a^3/3)$ and the linear stability of that fixed point is described in terms of the trace $\tau = 1 - a^2$ and the determinant $\Delta = \epsilon > 0$. Here, the fixed point is stable if $a^2 > 1$, and a limit cycle becomes stable in the range $-1 < a < 1$ as a result of a Hopf bifurcation [8] at $a = \pm 1$, where the fixed point merges with the critical points of the x -nullcline.

B. Canard transition to relaxation oscillations

Whenever the fixed point $x_0(a)$ of Eq. (6) comes close to a critical point $x_c(a)$ of the x -nullcline, a sudden transition to a large-amplitude relaxation oscillation becomes possible. This transition, which occurs as the control parameter a crosses a critical value $a_c(\epsilon)$, is referred to as a *canard* explosion or implosion, depending on whether the large-amplitude relaxation oscillation appears or disappears. For a brief review of the early literature on

canard explosions, see Ref. [9] and references therein. For a mathematical treatment, on the other hand, see Refs. [6, 11].

We now present a perturbative calculation of the critical canard parameter $a_c(\epsilon)$ as an asymptotic expansion in terms of the small parameter ϵ . For this purpose, we use the invariant-manifold solution $y = \Phi(x, \epsilon)$ of geometric singular perturbation theory [6, 7], which yields the generic canard perturbation equation

$$\begin{aligned} \dot{y} &= \epsilon G(x, \Phi(x, \epsilon); a) = \frac{\partial \Phi(x, \epsilon)}{\partial x} \dot{x} \\ &= \frac{\partial \Phi(x, \epsilon)}{\partial x} F(x, \Phi(x, \epsilon); a), \end{aligned} \quad (11)$$

where $\Phi(x, \epsilon) = \sum_{k=0}^{\infty} \epsilon^k \Phi_k(x)$ and $a_c(\epsilon) = \sum_{k=0}^{\infty} \epsilon^k a_k$. At the lowest order ($\epsilon = 0$), we find

$$0 = F(x, \Phi_0(x); a_0), \quad (12)$$

which yields the lowest-order x -nullcline

$$\Phi_0(x) \equiv f(x; a_0). \quad (13)$$

1. First-order perturbation analysis

At the first order in ϵ , we now find from Eq. (11):

$$G(x, \Phi_0; a_0) = \Phi'_0(x) [F_{y0} \Phi_1(x) + F_{a0} a_1], \quad (14)$$

where $F_{y0} = (\partial F / \partial y)_0 \neq 0$ and $F_{a0} = (\partial F / \partial a)_0$ are evaluated at $(x, \Phi_0; a_0)$. Here, $\Phi'_0(x)$ can be factored as

$$\Phi'_0(x) \equiv (x - x_c) \Psi_0(x), \quad (15)$$

where $\Psi_0(x)$ is assumed to be finite at the critical point $x = x_c(a_0)$ (i.e., a minimum or a maximum of the x -nullcline). Since the right side vanishes at the critical point $x_c(a_0)$, we find that $G(x_c, \Phi_{0c}; a_0) = 0$ implies the identity

$$x_0(a_0) \equiv x_c(a_0), \quad (16)$$

where the fixed point x_0 has merged with the critical point x_c of the x -nullcline at a unique value a_0 , i.e., the fixed point $x_0(a_0)$ is either at the maximum $x_0(a_0) = x_B(a_0)$, which yields $a_0 = a_{B0}$, or at the minimum $x_0(a_0) = x_D(a_0)$, which yields $a_0 = a_{D0}$. With this choice of a_0 , we can write the factorization

$$G(x, \Phi_0; a_0) \equiv (x - x_c) H_1(x), \quad (17)$$

where $H_1(x)$ is finite at $x = x_c(a_0)$.

Hence, from Eq. (14), we obtain the first-order solution

$$\Phi_1(x) \equiv K_1(x) - h(x) a_1, \quad (18)$$

where we introduced the definitions

$$\left. \begin{aligned} K_1(x) &\equiv H_1(x) / [\Psi_0(x) F_{y0}(x)] \\ h(x) &\equiv F_{a0}(x) / F_{y0}(x) \end{aligned} \right\}, \quad (19)$$

which are both finite at $x = x_c(a_0)$.

2. Second-order perturbation analysis

At the second order in ϵ , we find from Eq. (11):

$$\begin{aligned} G_{y0} \Phi_1 + G_{a0} a_1 &= \Phi'_0 \left(F_{y0} \Phi_2 + F_{a0} a_2 \right) \\ &+ \Phi'_1 \left(F_{y0} \Phi_1 + F_{a0} a_1 \right) \\ &= \Phi'_0 F_{y0} \left(\Phi_2 + h a_2 \right) \\ &+ F_{y0} \left(K'_1 - h' a_1 \right) K_1, \end{aligned} \quad (20)$$

where $G_{y0} = (\partial G / \partial y)_0$ and $G_{a0} = (\partial G / \partial a)_0$ are evaluated at $(x, \Phi_0; a_0)$, and we have used the first-order solution (18). By rearranging terms in Eq. (20), we obtain the second-order equation

$$S_1(x) a_1 - R_2(x) = \Phi'_0(x) \left[F_{y0} \Phi_2(x) + F_{a0} a_2 \right], \quad (21)$$

where we introduced the definitions

$$R_2(x) = K_1(x) \left[F_{y0} K'_1(x) - G_{y0} \right], \quad (22)$$

$$S_1(x) = G_{a0} - G_{y0} h(x) + F_{y0} h'(x) K_1(x), \quad (23)$$

which are both finite at $x_c(a_0)$.

Once again, since the right side of this equation vanishes at the critical point $x = x_c(a_0)$, the left side must also vanish at that point, and we obtain the first-order correction

$$a_1 = R_2(x_c) / S_1(x_c). \quad (24)$$

By factoring the left side of Eq. (21),

$$S_1(x) a_1 - R_2(x) = (x - x_c) H_2(x), \quad (25)$$

we now obtain the second-order solution

$$\Phi_2(x) \equiv K_2(x) - h(x) a_2, \quad (26)$$

where $K_2(x) \equiv H_2(x) / [\Psi_0(x) F_{y0}(x)]$ and $h(x)$ is defined in Eq. (19).

3. Higher-order perturbation analysis

By continuing the perturbation analysis at higher order ($n \geq 3$), Eq. (11) yields the n th-order equation

$$S_1(x) a_{n-1} - R_n(x) = \Phi'_0(x) F_{y0} [\Phi_n(x) + h(x) a_n], \quad (27)$$

where $S_1(x)$ is defined in Eq. (23) and

$$\begin{aligned} R_n(x) &= K_1(x) F_{y0} K'_{n-1}(x) - G_{y0} K_{n-1}(x) \\ &+ \sum_{k=1}^{n-2} F_{y0} [K'_k(x) - h'(x) a_k] K_{n-k}(x). \end{aligned} \quad (28)$$

Hence, the left side of Eq. (27) vanishes at x_c if

$$a_{n-1} = R_n(x_c) / S_1(x_c), \quad (29)$$

and the n th-order solution is obtained by first obtaining the factorization

$$S_1(x) a_{n-1} - R_n(x) = (x - x_c) H_n(x), \quad (30)$$

so that

$$\Phi_n(x) \equiv K_n(x) - h(x) a_n, \quad (31)$$

where $K_n(x) \equiv H_n(x) / [\Psi_0(x) F_{y0}(x)]$ and

$$a_n = R_{n+1}(x_c) / S_1(x_c), \quad (32)$$

is calculated from Eq. (28). We note that, once the function $R_n(x)$ is calculated in Eq. (28), the most computationally-intensive step is the factorization (30), with a_{n-1} calculated from Eq. (29).

As a result of the perturbative solution of Eq. (11), we have, therefore, calculated the perturbation expansion of the canard critical parameter

$$a_c(\epsilon) = a_0 + \frac{1}{S_1(x_c)} \sum_{k=1}^{\infty} \epsilon^k R_{k+1}(x_c). \quad (33)$$

For most applications, however, Eq. (33) can be truncated at first order in the asymptotic limit $\epsilon \ll 1$: $a_c(\epsilon) \simeq a_0 + a_1 \epsilon$, where $a_1 > 0$ for a canard explosion, while $a_1 < 0$ for a canard implosion.

4. Van der Pol canard perturbation analysis

Figure 3 shows that the biased Van der Pol equations (9) undergo canard explosion and implosion, when a small change in the bias parameter $a = -0.998740 \rightarrow -0.998739$ leads to the appearance of a large-amplitude relaxation oscillation from small-amplitude oscillations about the fixed point, while a small change in the bias parameter $a = 0.998739 \rightarrow 0.998740$ leading to the disappearance of large amplitude oscillations in $x(t)$ and $y(t)$ for the case $\epsilon = 0.01$.

The canard perturbation equation (11) for the Van der Pol equations (9) is

$$\epsilon \left[x - a(\epsilon) \right] = \frac{\partial \Phi(x, \epsilon)}{\partial x} \left[\Phi_0(x) - \Phi(x, \epsilon) \right], \quad (34)$$

where the partial derivatives evaluated at $\epsilon = 0$ are

$$\left. \begin{aligned} (F_{y0}, F_{a0}) &= (-1, 0) \\ (G_{y0}, G_{a0}) &= (0, -1) \end{aligned} \right\}. \quad (35)$$

Here, the lowest-order solution $\Phi_0(x) = x - x^3/3$ has critical points at $x_c = \pm 1$ where $\Phi'_0(x) = 1 - x^2$ vanishes. Hence, the lowest-order fixed point $x_0 = a_0$ merges with

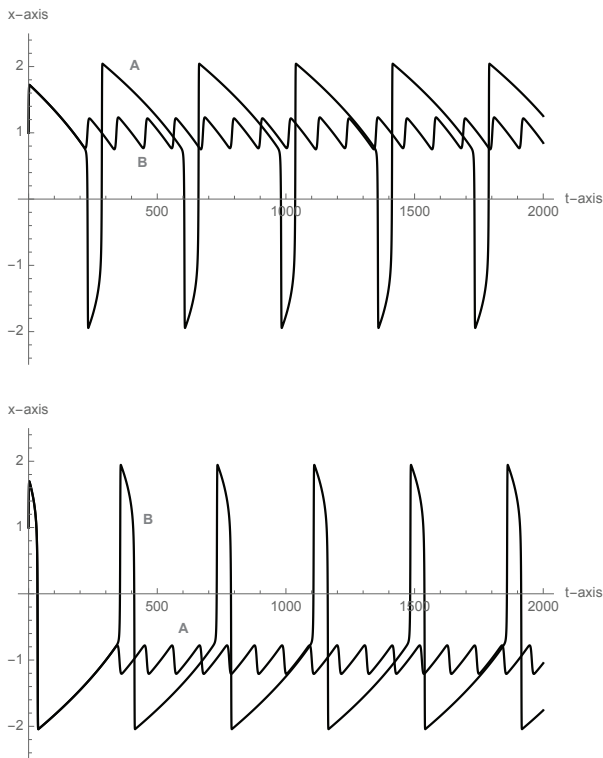


FIG. 3: Canard behavior in the Van der Pol equations for $\epsilon = 0.01$. (Top) Canard implosion when the large-amplitude relaxation oscillation suddenly disappears as $a = 0.998739$ (A) \rightarrow 0.998740 (B). (Bottom) Canard explosion when the large-amplitude relaxation oscillation suddenly appears as $a = -0.998740$ (A) \rightarrow -0.998739 (B).

the critical point x_c when $a_0 = \pm 1$. Because $F_{a_0} = 0$, the function $h(x) = 0$ in Eq. (19), while $\Psi_0(x) = x + a_0$ and $H_1(x) = -1$, so that $K_1(x) = 1/(x + a_0) = \Phi_1(x)$.

Next, in Eqs. (22)-(23), we have $R_2 = -K_1 K'_1 = 1/(x + a_0)^3$ and $S_1 = -1$, so that at $x = a_0 = \pm 1$, we find the first-order correction $a_1 = -1/(8 a_0^3)$, i.e., $a_1 = -1/8$ for the canard implosion at $a_0 = 1$, and $a_1 = 1/8$ for the canard explosion at $a_0 = -1$.

For the canard explosion, the calculated critical parameter (truncated at first order) $a_c(\epsilon) = -1 + \epsilon/8$ yields $a_c(0.01) = -0.99875$, which is in excellent agreement with the numerical value $-0.998740\dots$ shown in Fig. 3. Because of the symmetry of the Van der Pol model, the calculated critical parameter (truncated at first order) $a_c(\epsilon) = 1 - \epsilon/8$ for the canard implosion yields $a_c(0.01) = 0.99875$, which is again in excellent agreement with the numerical value $0.998740\dots$ shown in Fig. 3. Higher-order corrections to the Van der Pol canard parameter $a_c(\epsilon) = 1 - \epsilon/8 - 3\epsilon^2/32 - 173\epsilon^3/1024 - \dots$ can be computed up to arbitrary order [12] but they are not needed in what follows.

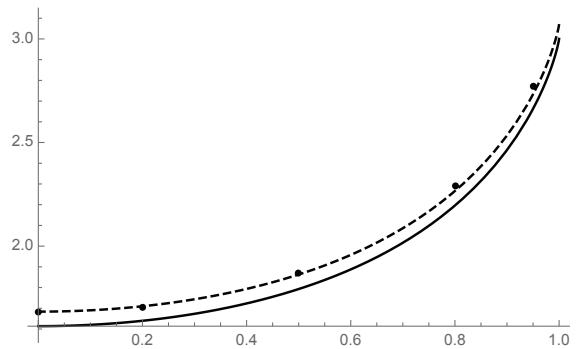


FIG. 4: Plots of the asymptotic Van der Pol period $\epsilon T_{\text{VdP}}(a)$ (solid) and the corrected asymptotic Van der Pol period $\epsilon T_{\text{VdP}}^\alpha(a, \epsilon)$ (dashed) versus the bias parameter a , in the limit $\epsilon = 0.001 \ll 1$. The numerical periods $\epsilon T_{\text{num}}(a, \epsilon)$, shown as dots, are approximately 4% higher than the asymptotic Van der Pol period (37) and are within 1% of the corrected asymptotic Van der Pol period (38).

C. Asymptotic limit-cycle period

We saw in Figs. 1-2 that, in the asymptotic limit $\epsilon \ll 1$, the limit-cycle curve of Eq. (6) is composed of slow segments that are close to the x -nullcline. In this limit, the asymptotic period can be calculated as follows. First, we begin with the x -nullcline $y = f(x; a)$ on which we obtain $dy/dt = f'(x; a) dx/dt$. Next, we use the y -equation $dy/dt = \epsilon G(x, y; a)$, into which we substitute the x -nullcline equation: $dy/dt = \epsilon G(x, f(x; a); a)$.

By combining these equations, we obtain the infinitesimal asymptotic-period equation

$$\epsilon dt = f'(x; a) dx / G(x, f(x; a); a),$$

which yields the asymptotic limit-cycle period

$$\epsilon T_{\text{ABCD}}(a) = \int_{x_A(a)}^{x_B(a)} \frac{f'(x; a) dx}{G(x, f(x; a); a)} + \int_{x_C(a)}^{x_D(a)} \frac{f'(x; a) dx}{G(x, f(x; a); a)}. \quad (36)$$

Here, the asymptotic limit cycle ABCDA combines the slow x -nullcline orbits $x_A \rightarrow x_B$ and $x_C \rightarrow x_D$ and the fast horizontal transitions $x_B \rightarrow x_C$ and $x_D \rightarrow x_A$, which are ignored in Eq. (36). Generically, the values $x_D(a) < x_B(a)$ are the minimum and maximum of the x -nullcline $y = f(x; a)$, respectively, where $f'(x; a)$ vanishes. The points $x_C(a) < x_A(a)$, on the other hand, are the minimum and maximum of the asymptotic limit cycle.

In the limit $\epsilon \ll 1$, the phase-space portrait for the Van der Pol equations (9) shown in Fig. 1 has slow segments $A(x_A = 2) \rightarrow B(x_B = 1)$ and $C(x_C = -2) \rightarrow D(x_D = -1)$ on the x -nullcline (shown as a dashed curve) and fast horizontal transitions $B(x_B = 1) \rightarrow C(x_C = -2)$ and $D(x_D = -1) \rightarrow A(x_A = 2)$. The asymptotic period (36)

for the Van der Pol limit-cycle ABCDA is calculated as

$$\begin{aligned} \epsilon T_{\text{VdP}}(a) &= \int_2^1 \frac{(1-x^2) dx}{x-a} + \int_{-2}^{-1} \frac{(1-x^2) dx}{x-a} \\ &= 3 - (1-a^2) \ln \left(\frac{4-a^2}{1-a^2} \right), \end{aligned} \quad (37)$$

which is shown in Fig. 4 as a solid curve. We note that the asymptotic Van der Pol period (37) is symmetric in a , i.e., $T_{\text{VdP}}(-a) = T_{\text{VdP}}(a)$.

The next term in the asymptotic expansion of the Van der Pol period (37) involves a nontrivial correction associated with the complex orbits seen in Fig. 2 on their way to the turning points at $x_{A,C} \simeq \pm 2$ [8]. This correction is expressed as $3\alpha\epsilon^{2/3}$ [13], where $\alpha = 2.338107\dots$ denotes the lowest zero of the Airy function $\text{Ai}(-x)$. If we add this correction to the Van der Pol asymptotic period (37), we obtain

$$\epsilon T_{\text{VdP}}^\alpha(a, \epsilon) \equiv 3 - (1-a^2) \ln \left(\frac{4-a^2}{1-a^2} \right) + 3\alpha\epsilon^{2/3}, \quad (38)$$

where the correction is assumed to be independent of the bias parameter a (a more thorough calculation, which is omitted here, would be required to explore this dependence).

The numerical periods $\epsilon T_{\text{num}}(a, \epsilon)$, which are shown in Fig. 4 as dots, are within 4% higher than the asymptotic Van der Pol period (37) and are within 1% of the corrected asymptotic Van der Pol period (38). These numerical results show that the asymptotic limit $\epsilon \ll 1$ enables us to evaluate the limit-cycle period according to Eq. (38) with excellent accuracy, on both qualitative and quantitative basis.

III. FITZHUGH-NAGUMO EQUATIONS

The FHN equations [3] offer a simple model used to study the conditions leading to firing of neuron cells. Here, the FHN equations are expressed as

$$\dot{x} = x - x^3/3 + c - y, \quad (39)$$

$$\dot{y} = \epsilon(x + a - by), \quad (40)$$

where (a, b, c) are constants and $\epsilon \ll 1$. In what follows, we will use the model parameters $(a, b) = (3/5, 4/5)$ for the purpose of explicit calculations and numerical simulations, and the control parameter c will determine the type of solutions for Eqs. (39)-(40).

The FHN nullcline equations are

$$\left. \begin{aligned} x - \text{nullcline} : f(x) &= x - x^3/3 + c \\ y - \text{nullcline} : g(x) &= (5x + 3)/4 \end{aligned} \right\}, \quad (41)$$

which intersect at a single fixed point (x_0, y_0) , where $x_0(c)$ is the single real root of the cubic equation

$$4x^3 + 3x - (12c - 9) = 0. \quad (42)$$

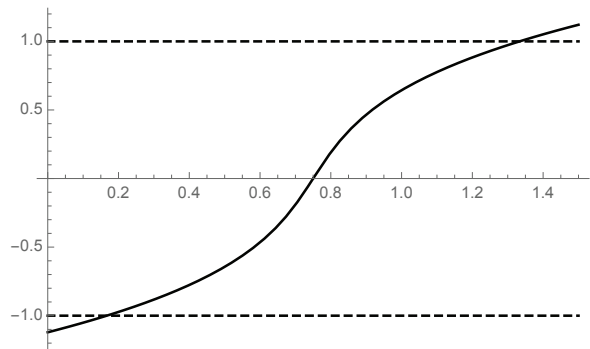


FIG. 5: Plot of the fixed point $x_0(c) = \sinh[\psi(c)/3]$ as a function of the control parameter c . The fixed point reaches the critical points ± 1 (dashed lines) of the x -nullcline at $c = 1/6$ and $c = 4/3$.

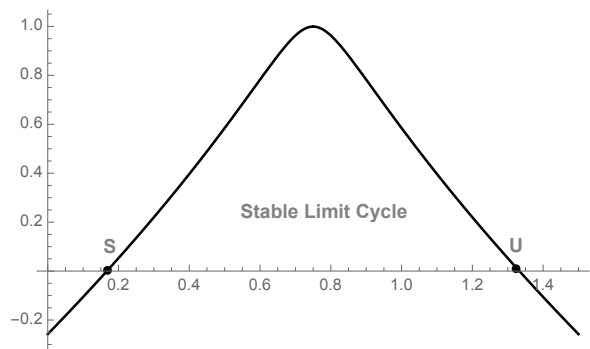


FIG. 6: Linear stability diagram for the FHN equations for $\epsilon = 0.001$. Trace $\tau(c)$ versus c , showing a stable limit cycle in the range $c_s(\epsilon) < c < c_u(\epsilon)$.

The three roots of this equation [14] are

$$x_1(c) = i \cos \left(\frac{\pi}{6} - i \frac{\psi(c)}{3} \right), \quad (43)$$

$$x_2(c) = -i \cos \left(\frac{\pi}{2} - i \frac{\psi(c)}{3} \right) = \sinh \left(\frac{1}{3} \psi(c) \right), \quad (44)$$

$$x_3(c) = -i \cos \left(\frac{\pi}{6} + i \frac{\psi(c)}{3} \right) \equiv x_1^*(c), \quad (45)$$

where $\psi(c) \equiv \text{arcsinh}(12c - 9)$. Here, the fixed point $x_0(c) = x_2(c) = \sinh[\psi(c)/3]$ reaches the critical points ± 1 of the x -nullcline at $c = 1/6$ and $c = 4/3$, respectively (see Fig. 5).

A. Linear stability of the fixed point

The linear stability of the fixed point (x_0, y_0) is determined from the Jacobian matrix

$$J_0(c, \epsilon) = \begin{pmatrix} 1 - x_0^2(c) & -1 \\ \epsilon & -4\epsilon/5 \end{pmatrix}, \quad (46)$$

where the trace is $\tau = (1 - 4\epsilon/5) - x_0^2$ and the determinant is $\Delta = \epsilon(1 + 4x_0^2)/5 > 0$. Marginal stability ($\tau = 0$)

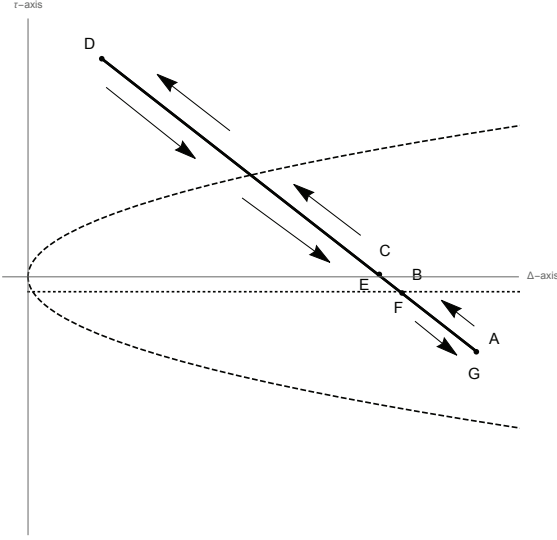


FIG. 7: Path in the stability (trace-versus-determinant) space for $0 \leq c \leq 3/2$. The dashed parabola denotes $\Delta(c) = \tau^2(c)/4$ and the horizontal dotted line at $\tau(c) = -4\epsilon/5$ represents the location where $x_0(c) = \pm 1$. The description of the path ABCDEFG is presented in the text.

occurs at $c_s(\epsilon) = 3/4 - \delta(\epsilon)/12$ and $c_u(\epsilon) = 3/4 + \delta(\epsilon)/12$, where $\delta(\epsilon) = (7 - 16\epsilon/5)\sqrt{1 - 4\epsilon/5} < 7$ for $\epsilon > 0$. Here, the fixed point is stable if $c < c_s(\epsilon)$ and $c > c_u(\epsilon)$, while a limit cycle is stable (for $\epsilon = 0.001$) in the range

$$c_s(\epsilon) = 0.167167 < c < c_u(\epsilon) = 1.33283. \quad (47)$$

Here, we note that $c_s(\epsilon) > 3/4 - 7/12 = 1/6$ and $c_u(\epsilon) < 3/4 + 7/12 = 4/3$, i.e., the fixed point loses stability after it has reached the x -nullcline minimum at $x = -1$, while it regains stability before it has reached the x -nullcline maximum at $x = 1$.

Figure 7 shows a path in the stability (trace-versus-determinant) space for $0 \leq c \leq 3/2$. The path begins at $c = 0$ (A), where the fixed point is stable ($\tau < 0$). As c increases, it first reaches $c = 1/6$ (B) where the fixed point is at the critical point $x_0 = -1$ of the x -nullcline. At $c = c_s(\epsilon) = 0.167167$ (C), the fixed point becomes marginally stable ($\tau = 0$). A Hopf bifurcation yields a stable limit cycle for $c > c_s(\epsilon)$ as we go through $c = 3/4$ (D) until we return to marginal stability at $c = c_u(\epsilon) = 1.33283$ (E). As c continues to increase, we reach $c = 4/3$ (F), when the fixed point is at the critical point $x_0 = +1$ of the x -nullcline, and then ultimately we return to the starting point of the path at $c = 3/2$ (G). We note that at point D ($c = 3/4$), the trace τ reaches its highest (positive) value, which corresponds to the fastest firing rate.

B. Canard behavior of the FHN Solutions

The singular canard perturbation equation (11) for the FHN equations (39)-(40) is

$$\epsilon(x + a - b\Phi) = \frac{\partial\Phi}{\partial x} \left(x - \frac{x^3}{3} + c - \Phi \right), \quad (48)$$

where $\Phi(x, \epsilon) = \sum_{k=0} \epsilon^k \Phi_k(x)$ and $c(\epsilon) = \sum_{k=0} \epsilon^k c_k$, and we use $(a, b) = (3/5, 4/5)$. Here, the partial derivatives evaluated at $\epsilon = 0$ are

$$\left. \begin{aligned} F_{y0} &= -1 \\ F_{c0} &= 1 \\ G_{y0} &= -b \\ G_{c0} &= 0 \end{aligned} \right\}. \quad (49)$$

At lowest order ($\epsilon = 0$), we find $\Phi_0(x) = x - x^3/3 + c_0$, which has two critical points at $x_c = \pm 1$.

At first order, we find

$$x + a - b\Phi_0(x) = \Phi'_0(x) \left(c_1 - \Phi_1(x) \right), \quad (50)$$

where the right side vanishes at the critical point $x = \pm 1$ of $\Phi_0(x)$. In order for $\Phi_1(x)$ to be regular at the critical points, we require the left side to also vanish at $x = \pm 1$. Hence, we find $12c_0^\pm - 9 = \pm 7$, which yields $c_0^+ = c_u(0) = 4/3$ at $x_c = +1$ and $c_0^- = c_s(0) = 1/6$ at $x_c = -1$. By factoring both sides by $x \mp 1$, we find

$$H_1^\pm(x) = -\Psi_0^\pm(x) \left(c_1 - \Phi_1(x) \right),$$

where $H_1^\pm(x) = (4x^2 \pm 4x + 7)/15$ and $\Psi_0^\pm(x) = (x \pm 1)$. Hence, the first-order solution is

$$\Phi_1(x) = c_1 + K_1(x), \quad (51)$$

where $K_1(x) = (4x^2 \pm 4x + 7)/[15(x \pm 1)]$.

At the second order, we find

$$-(4/5)\Phi_1 = \Phi'_0(c_2 - \Phi_2) + \Phi'_1(c_1 - \Phi_1),$$

which can be expressed as

$$R_2(x) - (4/5)c_1 = \Phi'_0(x) \left(c_2 - \Phi_2(x) \right), \quad (52)$$

where $R_2(x) = K_1(x)[K'_1(x) - 4/5]$. Once again, since the right side vanishes at the critical point $x = \pm 1$ of $\Phi_0(x)$, we require that $c_1^\pm = R_2(\pm 1)/b = \mp 13/32$.

Hence, when truncated at first order in ϵ , the canard explosion and implosion occur at

$$\left. \begin{aligned} c^-(\epsilon) &= 1/6 + 13\epsilon/32 = 0.167073 \\ c^+(\epsilon) &= 4/3 - 13\epsilon/32 = 1.33293 \end{aligned} \right\}, \quad (53)$$

respectively, where we used $\epsilon = 0.001$. These values agree very well with the numerical results shown in Fig. 8. We note that the canard explosion occurs between points B ($c = 1/6$) and C ($c = c_s$) in Fig. 7, while the canard implosion occurs between points E ($c = c_u$) and F ($c = 4/3$), i.e., these canard events occur between marginal stability and the fixed point located at the critical points ± 1 of the x -nullcline.

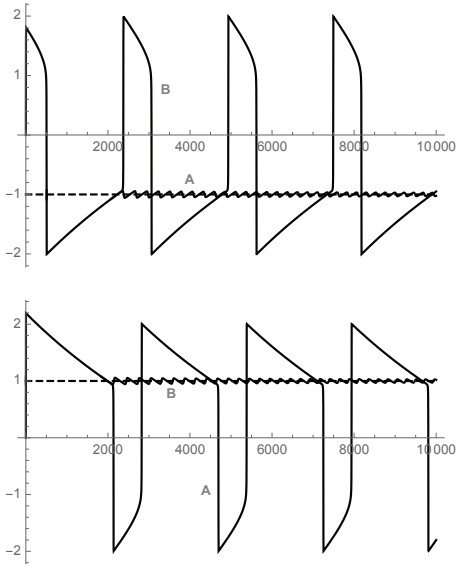


FIG. 8: Canard behavior in the FHN equations for $\epsilon = 0.001$ with initial conditions $(x, y) = (0, 0)$. (top) Canard explosion $c = 0.16707$ (A) \rightarrow 0.16708 (B) (bottom) Canard implosion $c = 1.33292$ (A) \rightarrow 1.33293 (B).

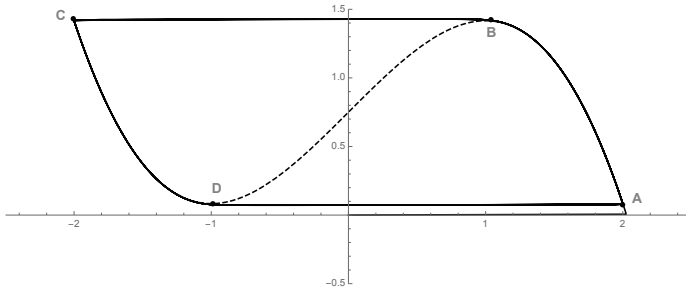


FIG. 9: Asymptotic limit cycle $ABCD A$ for the FHN equations, for $c = 3/4$ and $\epsilon = 0.001 \ll 1$. The slow segments A ($x = 2$) \rightarrow B ($x = 1$) and C ($x = -2$) \rightarrow D ($x = -1$) lie on the x -nullcline, while the transitions $B \rightarrow C$ and $D \rightarrow A$ are fast.

C. Asymptotic limit-cycle period

Using the numerical solutions shown in Figs. 9-10, we see that the segments A ($x = 2$) \rightarrow B ($x = 1$) and C ($x = -2$) \rightarrow D ($x = -1$) on the x -nullcline occur on a much longer time scale than the fast transitions $B \rightarrow C$ and $D \rightarrow A$.

We now construct the asymptotic limit-cycle integral (36) with the x -nullcline equation $y = x - x^3/3 + c$, which yields $\dot{y} = (1 - x^2)\dot{x}$, and the y -equation $\dot{y} = \epsilon(x + a - by)$ evaluated on the x -nullcline: $\dot{y} = \epsilon[x + a - b(x - x^3/3 + c)]$.

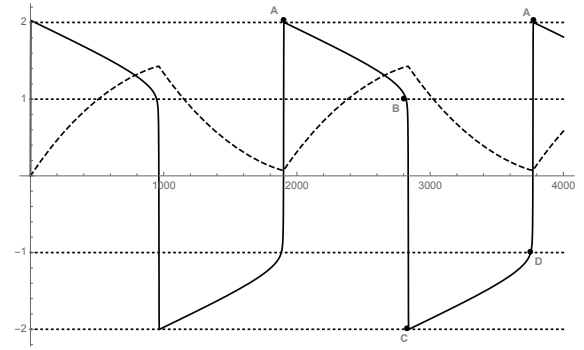


FIG. 10: FitzHugh-Nagumo solutions $x(t)$ (solid) and $y(t)$ (dashed) for $c = 3/4$ and $\epsilon = 0.001$.

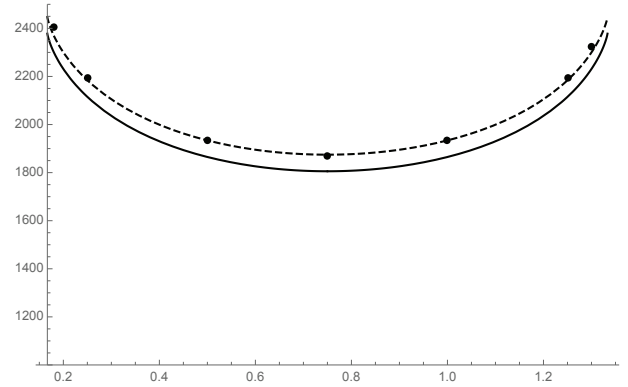


FIG. 11: Plots of the asymptotic FHN period $T_{\text{FHN}}(c)$ (solid) and the corrected asymptotic FHN period $T_{\text{FHN}}^\alpha(c, \epsilon)$ (dashed) versus c for $\epsilon = 0.001$. Numerical periods (shown as dots) are all within 4% above the function $T_{\text{FHN}}(c)$, while they are within 1% of the corrected period $T_{\text{FHN}}^\alpha(c, \epsilon)$.

We then obtain the infinitesimal equation

$$\begin{aligned} \epsilon dt &= \frac{(1 - x^2) dx}{[bx^3/3 + (1 - b)x - (bc - a)]} \\ &= \frac{(3/b)(1 - x^2) dx}{(x - x_1)(x - x_2)(x - x_3)}, \end{aligned} \quad (54)$$

where $x_1(c) = x_3^*(c)$ and $x_2(c)$ are the roots defined in Eqs. (43)-(45).

The asymptotic limit-cycle period for the FHN equations is thus given by the integrals

$$\begin{aligned} \epsilon T_{\text{FHN}}(c) &= \frac{3}{b} \int_2^1 \frac{(1 - x^2) dx}{(x - x_1)(x - x_2)(x - x_3)} \\ &+ \frac{3}{b} \int_{-2}^{-1} \frac{(1 - x^2) dx}{(x - x_1)(x - x_2)(x - x_3)}. \end{aligned} \quad (55)$$

We now introduce the partial-fraction decomposition

$$\frac{(1 - x^2)}{(x - x_1)(x - x_2)(x - x_3)} = \frac{p_1}{x - x_1} + \frac{p_2}{x - x_2} + \frac{p_3}{x - x_3},$$

with the coefficients

$$p_1(c) = -\frac{(x_2 - x_3)}{\Delta} \left(1 - x_1^2\right), \quad (56)$$

$$p_2(c) = -\frac{(x_3 - x_1)}{\Delta} \left(1 - x_2^2\right), \quad (57)$$

$$p_3(c) = -\frac{(x_1 - x_2)}{\Delta} \left(1 - x_3^2\right), \quad (58)$$

where $\Delta = (x_1 - x_2)(x_2 - x_3)(x_3 - x_1)$ and we used $x_1 + x_2 + x_3 = 0$. Hence, Eq. (55) can be written as

$$\epsilon T_{\text{FHN}}(c) = -\frac{3}{b} \sum_{k=1}^3 p_k \ln \left(\frac{4 - x_k^2}{1 - x_k^2} \right). \quad (59)$$

If we add the same nontrivial Van der Pol correction $3\alpha\epsilon^{2/3}$ [see Eq. (38)] to the asymptotic FHN period (59), we can define the corrected period

$$T_{\text{FHN}}^\alpha(c, \epsilon) \equiv T_{\text{FHN}}(c) + 3\alpha/\epsilon^{1/3}. \quad (60)$$

Figure 11 shows that the exact numerical periods (shown as dots) are all within 4% above the period $T_{\text{FHN}}(c)$,

while they are within 1% of the α -corrected period $T_{\text{FHN}}^\alpha(c, \epsilon)$.

IV. SUMMARY

In the present paper, we have shown how the asymptotic limit-cycle properties of the FHN equations (4)-(5) can be accurately calculated. Indeed, we have shown in Sec. IIIB how the singular perturbation theory of Fenichel [6] can be used to accurately predict the appearance (canard explosion) and disappearance (canard implosion) of large-amplitude relaxation oscillations (see Fig. 8) in the FHN equations (4)-(5). In addition, once large-amplitude relaxation oscillations are excited, the period of these oscillations can be accurately calculated in Eq. (59), where explicit formulas for the cubic roots (43)-(45) of the polynomial (42). The accuracy of Eq. (60) is clearly demonstrated in Fig. 11 when the nontrivial Van der Pol correction $3\alpha\epsilon^{2/3}$ is added to the FHN period (59).

-
- [1] R. FitzHugh, *Biophys. J.* **1**, 445 (1961).
 [2] J. Nagumo, S. Arimoto, and S. Yoshizawa, *Proceedings of the IRE* **50**, 2061 (1962).
 [3] E. M. Izhikevich and R. FitzHugh, *FitzHugh-Nagumo model*, *Scholarpedia* **1**, 1349 (2006).
 [4] A.L. Hodgkin and A.F. Huxley, *J. Physiol.* **117**, 500 (1952).
 [5] T. Kanamaru, *Van der Pol Oscillator*, *Scholarpedia* **2**, 2202 (2007).
 [6] N. Fenichel, *J. Diff. Eqs.* **31**, 53 (1979).
 [7] J.-M. Ginoux and J. Llibre, *J. Phys. A: Math. Theor.* **44**, 465203 (2011).
 [8] S. H. Strogatz, *Nonlinear Dynamics and Chaos*, 2nd ed. (Westview Press, 2015).
 [9] M. Diener, *Math. Intell.* **6**, 38 (1984).
 [10] In its standard dimensionless form [8], the Van der Pol equation is expressed in terms of the time coordinate normalized to the frequency ω , which means that Eq. (8) is expressed as $x'' - \epsilon(1 - x^2)x' + x = a$, where $\epsilon \equiv \nu/\omega \gg 1$. Hence, our small parameter is $\epsilon \equiv \epsilon^{-2} \ll 1$ and the non-standard correction is $3\alpha\epsilon^{2/3} = 3\alpha/\epsilon^{4/3}$.
 [11] M. Krupa and P. Szmolyan, *J. Diff. Eqs.* **174**, 312 (2001).
 [12] A. Algaba, K.-W. Chung, B.-W. Qin, and A.J. Rodríguez-Luis, *Physica D* **406**, 132384 (2020).
 [13] C.M. Bender and S.A. Orszag, *Advanced Mathematical Methods for Scientists and Engineers* (Wiley, 1978).
 [14] For the general solution for the roots of a cubic polynomial, see Appendix A of A.J. Brizard, *An Introduction to Lagrangian Mechanics*, 2nd ed. (World Scientific Press, 2014).